Electrical Conductance Map for the Kachchh Rift Basin: Constraint on Tectonic Evolution and Seismotectonic Implications

P. B. V. Subba Rao, B. R. Arora & A. K. Singh

Pure and Applied Geophysics
pageoph

ISSN 0033-4553
Volume 171
Number 9

Pure Appl. Geophys. (2014)
171:2353-2370
DOI 10.1007/s00024-014-0846-3

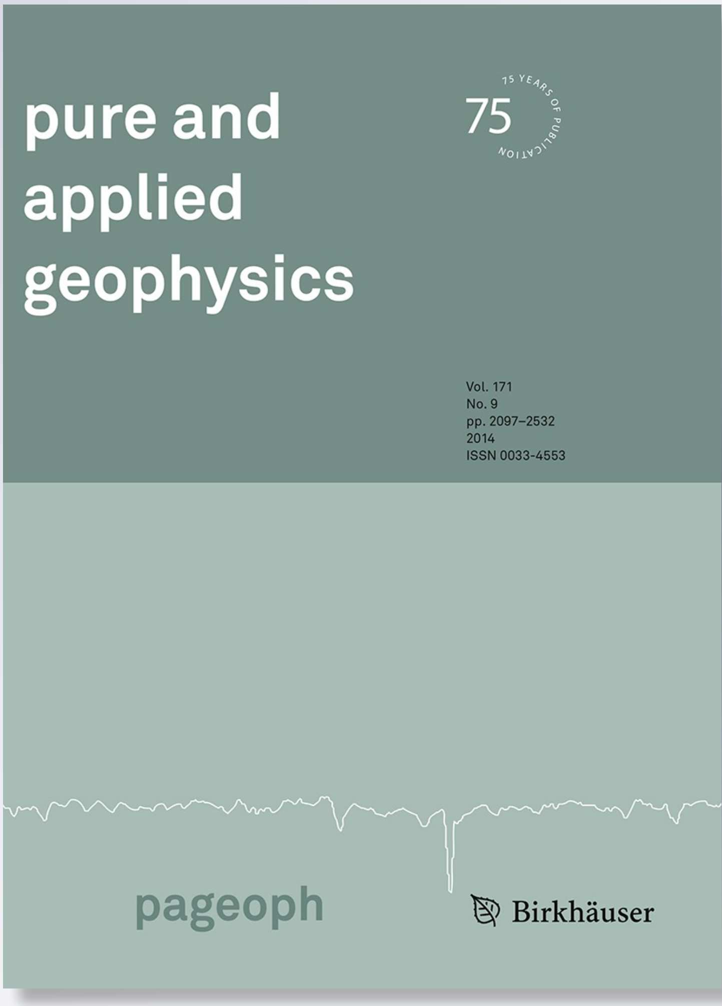

Pure Appl. Geophys. 171 (2014), 2353–2370
© 2014 Springer Basel
DOI 10.1007/s00024-014-0846-3

Pure and Applied Geophysics

Electrical Conductance Map for the Kachchh Rift Basin: Constraint on Tectonic Evolution and Seismotectonic Implications

P. B. V. Subba Rao,[1] B. R. Arora,[2,3] and A. K. Singh[1]

Abstract—Geomagnetic field variations recorded by an array of magnetometers spread across the Kachchh Rift basin are reduced to a set of induction arrows as a diagnostic of lateral electrical conductivity variations. A non-uniform thin-sheet electrical conductance model is developed to account for the salient induction patterns. It indicates that the imaged conductivity anomalies can be related to the sediment-filled structural lows in between the fault bounded uplifts. It is suggested that sagging structural lows preserved the marine sediments deposited during the Mesozoic sea transgression and later developed into first order embayment basins for the deposition of sediments in association with Late Eocene transgression. Depth integrated electrical conductance helped in mapping two depo-centres: along the ENE-WSW trending Banni half-Graben bounded by the Kachchh Main fault on the south and, second, along the Vinjan depression formed in response to the subsidence between the Vigodi fault and westward extension of the Katrol Hill fault together with the westward bending of the Median High. Presence of metamorphosed graphite schist clasts in shale dominated Mesozoic sequence and/or thin films of carbon resulting from the thermal influence of Deccan activity on Carbonate-rich formations can account for the high electrical conductivity anomalies seen in the depo-centres of thick Mesozoic and Tertiary sediments. Additionally two high conductivity zones are imaged encompassing a block defined by the 2001 Bhuj earthquake and its aftershocks. In agreement with gravity, magnetic and seismic velocity signatures, aqueous fluids released by recrystallizing magmatic bodies intruded in association with Deccan trap activity account for mapped high conductivity zones. High fluid pressure in such a fractured domain, surrounding the intruded magmatic plugs, perturb the regional stress concentrations to produce frequent and low magnitude aftershocks in the shallow section of the epicentral track of the 2001 Bhuj earthquake.

Key words: Rift basin, Mesozoic sediments, geomagnetic induction, electrical conductivity, fluid induced seismicity.

[1] Indian Institute of Geomagnetism, Panvel, Navi Mumbai 410218, India. E-mail: srao@iigs.iigm.res.in

[2] Uttarkhand State Council for Science and Technology, Dehradun 248001, India.

[3] *Present Address*: Division of Seismology, Ministry of Earth Sciences, Lodhi Road, New Delhi 110003, India.

1. Introduction

The Kachchh along with the Cambay and Narmada Basins on the western continental margin of India are the classical examples of the rift basins developed by the reactivation of the Precambrian trends following the breakup of Gondwana in the Late Triassic (Fig. 1). The NE-SW trending Delhi-Aravalli Precambrian orogenic belt swings E–W at its southern fringe and extends across the entire Kachchh region as the basement of the rift basin (Fig. 1). Reactivation of the basement faults along this regional Precambrian trend controlled the alignment of geomorphic subdivisions and major faults of the Kachchh Rift basin (KRB) and its subsequent evolution (Fig. 2a). The KRB has a long record of sedimentation history ranging from the Mesozoic to Tertiary/Recent. The regional tectonic framework, structures, sedimentation history and geotectonic evolution of the KRB are extensively discussed by Biswas (1982, 1987, 2005). The stages of sedimentations are time synchronous with events of sea transgression-regression related to sea floor spreading accompanying migration of the Indian plate. A Late Cretaceous tectonic event caused uplift of fault bounded blocks followed by large scale volcanic activity and wide spread magmatic intrusions. The on-going collision of India with Eurasia since the Tertiary is largely responsible for the present day landscape. Located around 1,000 km from the India–Eurasia plate boundary and 300–500 km from the western collision boundary along Chaman fault, the KRB has a long history of seismicity. The most notable among them are the 1819-Kachchh, 1956-Anjar and more the recent 2001-Bhuj earthquakes (Fig. 2a). The Bhuj earthquake with its epicenter at 23.4°N, 70.3°E and focal depth of

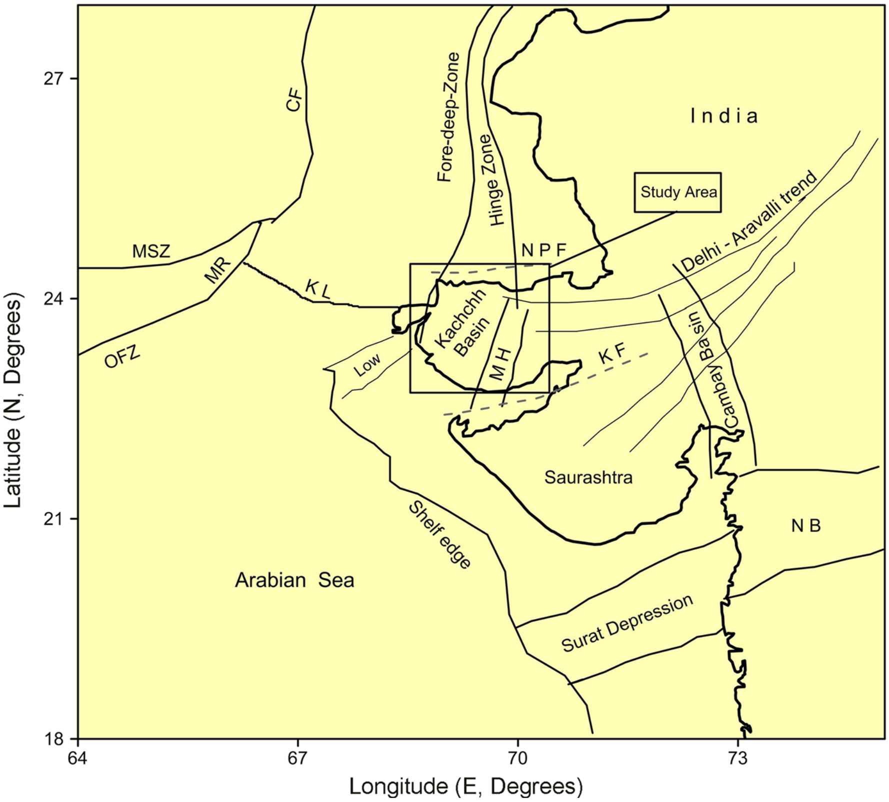

Figure 1

Map showing location of the Kachchh Rift basin in relation to the tectonic elements of the western continental margin and triple plate boundaries in the offshore region (modified from Biswas 1987; Kukowski *et al*. 2001). Kachchh–Lakhpat (KL) Lineament is considered link of Owen Fracture Zone (OFZ) and Murray Ridge (MR) with the KRB (Mishra *et al*. 2005) via the bathymetry 'LOW' (after Talwani and Gangopadhyay 2001). Box in the centre defines the area of the KRB, shown in enlarged form in Fig. 2

$\sim$25 km is considered a strong intraplate seismic event in the Indian shield (Gupta *et al*. 2001; Kayal *et al*. 2002a). The other recent examples of intraplate seismicity are the 1993 Latur earthquake and 1997 Jabalpur Earthquake (Kayal 2007). Multi-geophysical, seismological investigations undertaken in the aftermath of these earthquakes have suggested that the intraplate seismic activity may be related to the reactivation of pre-existing faults, intersecting faults or in situ material heterogeneities in response to stresses transmitted from the collision of Indian-Eurasian plates (Gowd *et al*. 1996; Bilham *et al*. 2003). Inversion of travel times of local earthquakes, using the principles of tomography, has imaged a fluid-filled low velocity zone engulfing the hypocenter block of a high velocity layer. The latter symbolises deep lithosphere melting forming an ultramafic magmatic body below KRB during rifting in early Jurassic ($\sim$160 Ma) and plume related volcanic activity during rift inversion in Late Cretaceous. It is suggested that the compact and strong crystallized magmatic body could have served as a repository of high stresses during earthquake build up cycle wherein the fluid pressure in the fractured mafic rock matrix above in the low velocity zone could have played a key role in the earthquake generating process (Kayal *et al*. 2002b; Mishra and Zhao 2003; Mandal *et al*. 2004; Biswas 2005; Mandal and Chadha 2008; Kayal 2010; Mandal 2012).

Given the sensitivity of electrical resistivity to fluids-filled porosity, the resistivity images serve as useful guide for the fluid distribution in the crust. The latter influence the mechanical and shear strength of the crustal rocks and, thus, control the rheology of the medium (Byerlee 1990; Cox 2005). It has been evidenced by the magnetotelluric (MT) investigations

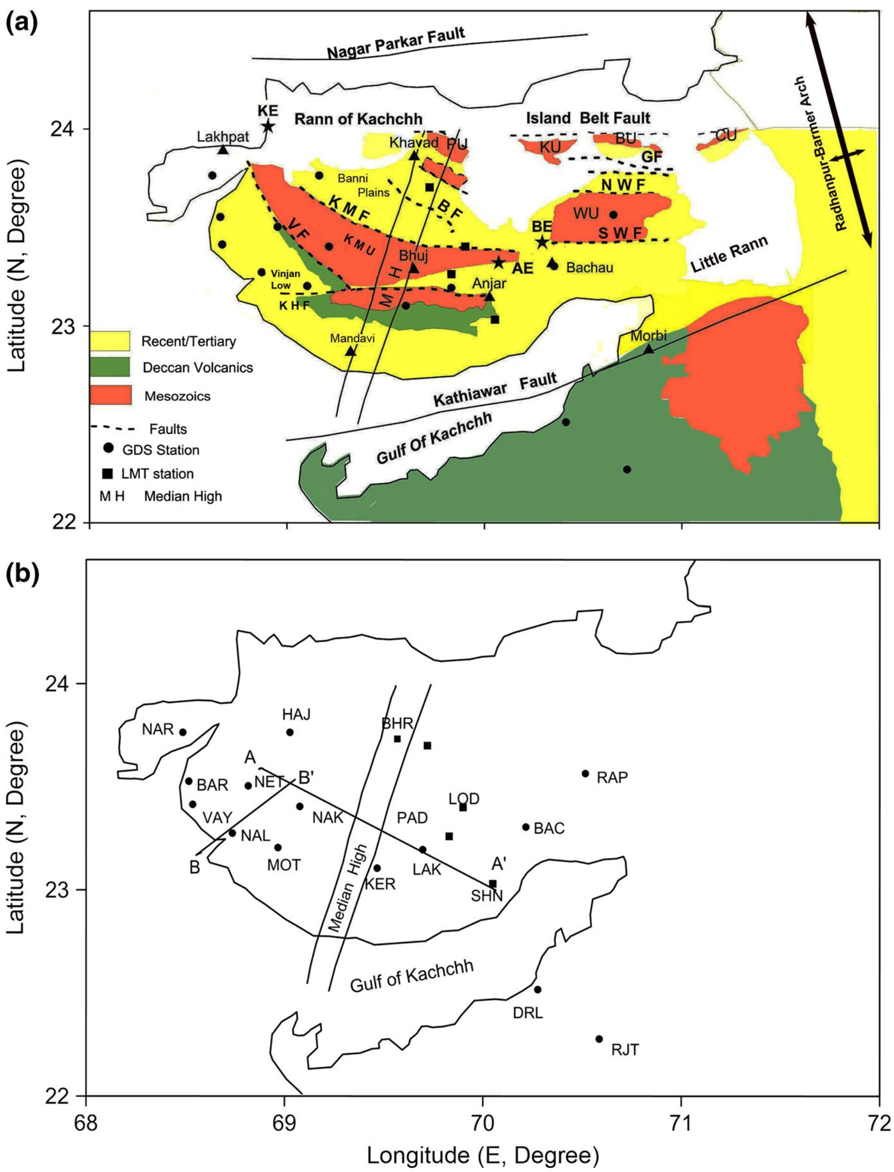

Figure 2

a Map of the Kachchh Rift Basin showing geology and major faults (modified from Biswas 1987; Mishra *et al*. 2005). Bounded to the north by the Nagar Parkar Fault and the Kathiawar Fault to the south, The KRB is dominated by several uplands (*KMU* Kachchh mainland uplift, *WU* Wagad uplift, and a chain of small uplands along the Island Band fault (IBF). Major faults are *KMF* Kachchh Mainland fault, *VF* Vigodi fault, *KHF* Katrol Hill fault, *SWF*, *NWF* South and North Wagad faults, *BF* Banni fault, *GF* Gedi fault). The epicentres of the 2001 Bhuj (BE), 1956 Anjar (AE) and 1819 Kachchh (KE) earthquakes are also marked. *Black circles* and *squares* mark GDS and LMT sites covered under the present study. **b** Location of GDS and LMT sites covered under the present study together with station codes referred to in the text. AA′ and BB′ are the profiles referred to in Fig. 4

that hypocenters of the Bhuj main shock and aftershocks were concentrated on the rheological boundary demarcated by the zones of contrasting high-low resistivity (Chandrasekhar *et al*. 2012). Given this proven efficacy of natural electromagnetic method in imaging the deep structures in the sediment filled environment of the KRB, the present work deals with a Geomagnetic Depth Sounding (GDS) experiment, a variant to MT method, which is well suited to map the structures marked by large lateral electrical conductivity (reciprocal of resistivity) contrast (Schmucker 1970; Beamish 1977; Arora 1997). The potential of GDS in imaging volcanic bodies and plutonic plugs has been well documented in one of the early studies in the basalt covered region of Valsad, near the western continental margin of India, which experienced a swarm type of seismic activity for a short interval (Arora and Reddy 1991). The present GDS experiment was initiated soon after the 2001 Bhuj earthquake as a part of a multi-disciplinary program launched to image structures in and around the epiceneral track (IIG Working Group 2002). In subsequent phases, the geographical coverage was expanded to cover as much large area of the KRB as permitted by logistics (Fig. 2a, b). The interpretation of the electrical conductivity distribution reduced from this regional-scale study has enabled some new insight on the tectonic evolution of the KRB as well as to place new constraints on the seismotectonic model for the Bhuj earthquake. With an objective to understand the origin of mapped conductive structures in the back drop of the evolution history of the KRB, key sequential stages involved in evolution of the basin are first reviewed. Next the principles of GDS, data acquisition, processing and modeling steps of time-varying magnetic fields collected from the KRB are briefly outlined. The factors responsible for enhanced electrical conductivity, the tectonic and seismotectonic implications of the imaged lateral conductivity distributions are then discussed in detail.

2. *Geology and Tectonics of the Kachchh Region*

The KRB on the western continental margin is a result of the break-up of Africa from Greater India from erstwhile Gondwanaland during Middle Jurassic (Biswas 1987 and references therein). Figure 1 shows the location of the KRB in a regional tectonic framework of western India whereas major geological and tectonic elements of the KRB are shown in Fig. 2a. Tectonic evolution of the basin commenced with the subsidence of a block between the sub-vertical Nagar Parkar and North Kathiawar faults, respectively, on the north and south of the block. The rifting progressed in stages by latitudinal faulting on a series of sub-parallel faults following the primordial E–W tectonic trend (Fig. 2a). The major faults from north to south include Allah Bund fault, Island Belt fault (IBF), Kachchh Mainland fault (KMF) and Katrol Hill fault (KHF). KHF continues westward into the offshore region to terminate at the flank of the Vinjan anticline whereas another segment of the KHF branches off to extend as a NW–SE trending Vigodi fault. The south-dipping Kathiawar fault defines the present day southern bounding fault of the basin. The rifting was aborted by the Late Cretaceous when KRB got filled with sediments of varying thicknesses (3–5 km) ranging in age from Middle Jurassic to Early Cretaceous (Biswas 1987, 2005; Talwani and Gangopadhyay 2001; Biswas and Khattri 2002; Mishra *et al*. 2005). Much of the sedimentation took place during syn-rift climax (Middle to Upper Jurassic) followed by post-rift regressive sedimentation in the Early Cretaceous. During the later phase, a thick sequence of Mesozoic marine and deltaic sediments (>3,000 m) was deposited in association with a major cycle of sea transgression/regression cycle. Late Cretaceous marks the most active tectonic phase in the evolution of the basin initiating the rift inversion phase that is continuing into the present neo-tectonic cycle. During this phase, thick piles of Mesozoic sediments were uplifted, folded, and intruded by mafic igneous rocks from a deep mantle source formed during syn-rift lithospheric melting, followed by large-scale Deccan Trap Basaltic flows from the Deccan plume. The uplifts where Mesozoic sediments are exposed were controlled by faults. Several small uplifts on the northern part of the basin are aligned on one side by IBF. The biggest Kachchh Mainland Uplift (KMU) occupying the central part of the basin is tilted to the south between KMF and NKF master-faults on the north and south, respectively. The Wagad uplift located northeast of the KMU is bounded by E–W oriented faults, South and North Wagad faults (SWF and NWF, Fig. 2a). The rift basin attained its present landscape during this stage where highlands distinguish areas of uplifts and surrounding low lying plains (Rann of Kachchh, Banni Plains, Coastal belt of Gulf of Kachchh) formed sub-basins for subsequent deposition during the post-rift sag stage beginning with Early Eocene transgression and subsequent Tertiary/Quaternary transgeresive-regressive cycles. Structurally, these sediment fill lows between uplifts are seen as half-grabens between tilted uplifts. As seen in Figs. 1 and 2a, the NNE–SSW trending Median High (MH) in the middle of the basin is the most prominent feature in the otherwise E–W dominated structures.

3. GDS Experiment, Methodology, Data Acquisition and Processing

3.1. Design of Field Experiment

In GDS, deduction of lateral conductivity distribution relies upon the time-varying geomagnetic field variations in three orthogonal components, viz, the geographic north (X), east (Y) and vertical (Z) components. Therefore, to map geoelectric structures of the KRB, basic time-varying geomagnetic field variations were recorded by operating fluxgate magnetometers at 14 sites (Fig. 2a, b). The regional coverage with inter-station spacing of 20–40 km was achieved by operating magnetometers successively in three different phases. In each phase, 4–7 fluxgate magnetometers were deployed to record variations in X, Y and Z with sampling interval of 30 s for a period of at least six weeks. In addition, the magnetic variations from four sites, where long period magnetotelluric (LMT) measurements were carried out, were also incorporated in the GDS analysis (Arora *et al*. 2002). The overall station's distribution provided coverage over all major tectonic blocks of the KRB.

3.2. Working Principle of GDS

The time-varying magnetic fields with their origin in the current systems in the ionosphere and distant magnetosphere act as a natural source of electromagnetic (EM) field and induce secondary currents in the conductive layers of the earth. The depth (δ) penetration of the induced currents is controlled by the well known skin-depth relation expressed as $\delta = 0.5\sqrt{(\rho \ T)} = 0.5\ \sqrt{(1/\sigma f)}$ km, here ρ ($1/\sigma$) is the resistivity- Ω m (conductivity, S/m) of the substratum and f (i.e., $1/T$) is frequency (period, T) in Hz (s). In theory, the ratios of internal to external parts over a range of frequencies are a primary diagnostic of conductivity distribution with depth. But given the limited spatial extent of the observational domain, much smaller than the spatial wavelength of the source currents, separation of the observed variations into external and internal parts is generally less satisfactory to infer conductivity distribution. Hence, in GDS, the fields are decomposed into normal and anomalous parts. The normal field components (X_n, Y_n, Z_n) are defined as the vector sum of magnetic fields due to the external current system and part of internal fields resulting from induction in the geoelectric model for the study region where conductivity varies only as a function depth (1-D). The anomalous parts (X_a, Y_a, Z_a) are entirely due to induction in the lateral electrical inhomogeneities. Identification and characterization of the anomalous parts is facilitated by the following physical rationales: (i) the external and internal constituents of the normal magnetic field reinforce each other in horizontal components but annul each other in case of a vertical magnetic field component (ii) the extensively large spatial wavelength of the external source fields, several thousand km, permits plane wave approximation for EM source fields. A net consequence of the above two factors is that (i) $X_n \gg X_a$; $Y_n \gg Y_a$ and (ii) Z_n is almost negligible over a layered earth. First approximation permits one to adopt observed X and Y variation to be a measure of normal fields (X_n and Y_n). Since the anomalous vertical fields are superposed on the nearly vanishing vertical field ($Z_n \approx 0$), the observed Z variations ($Z_a = Z$) signify signatures of induction in lateral conductivity inhomogeneity. This property of the Z is much exploited in the GDS to detect and map structures marked by strong lateral electrical conductivity contrast.

In addition to this preliminary diagnostic in time domain, much of the GDS data processing and interpretation proceeds by estimating frequency-dependent vertical field transfer functions (T_{ZX} and T_{ZY}). The later summarizing the relationship between the Fourier transform of vertical field component (measure of anomalous fields) and horizontal field components (reckoned to define characteristic of inducing EM fields) is expressed as follows at any given angular frequency ($\omega = 2\pi f$):

$$Z(\omega) = T_{ZX}(\omega)\,X(\omega) + T_{ZY}(\omega)\,Y(\omega), \quad (1)$$

where, $X(\omega)$, $Y(\omega)$ and $Z(\omega)$ are the Fourier transforms of north, east and vertical components of the geomagnetic field variations at the specified frequency. The transfer functions T_{ZX} and T_{ZY} are functions of electrical conductivity distribution at the observing site (SCHMUCKER 1970; BEAMISH 1977; ARORA 1997). These transfer functions are combined so as to obtain the magnitude (S) and direction (ϕ) of induction arrow is given by

$$S = \left(T_{ZX}^2 + T_{ZY}^2\right)^{0.5} \phi = Tan^{-1}(T_{ZY}/T_{ZX}). \quad (2)$$

It is usual to reverse the direction of the induction arrow so that it points towards region of high internal electrical conductivity (LILLEY and ARORA 1982). The transfer functions are complex numbers, and; hence, at the frequency in question define a pair of induction arrows, corresponding respectively to real and quadrature parts. A pair of induction arrows, when displayed on the geographic grid of stations, constitutes a powerful tool to locate the involved conductivity structure. The real induction arrows by way of their orientations define the strike, their magnitude, spatial decay pattern and frequency dependence contain information on the electric and geometrical parameters of the embedded structure. The quadrature part being sensitive to the phase difference in inducing and induced fields is a sensitive pointer to whether the induction is determined by resistance or inductance of the medium.

3.3. Data Selection and Estimation of Transfer Functions

The daily variations in geomagnetic fields have their origin in the ionosphere and its Fourier constituents do not satisfy the plane wave approximation, implicit in GDS formulation. During night-time when ionospheric contributions tend to be negligible, the magnetic variations are primarily associated with magnetospheric processes and, thus, fulfill quasi-uniform character of the source field. Therefore, only night-time segments, each of 8.5 h centered at local midnight, were used to compute period-dependent transfer functions. From the total recorded data, some 10–20 segments based on their large amplitude, wide frequency content and varied polarization were selected. The Fourier transforms of each segment was decimated at three levels by a factor of 4 so that a fixed 128-point FFT window allowes estimation of FT for each representative frequency band. Finally the transfer functions (Eq. 1) were computed using cross-spectral approach as defined by BEAMISH (1977). Overall transfer functions were computed for 13 bands in the period range of 8–128 min, the lower limit determined by rate of sampling and sensitivity of the magnetometers employed while the period of upper band was restricted so that variations validate approximation of a plane wave. Three sets of real and quadrature induction arrows for all stations covered under the present experiment in the KRB are shown in Fig. 3 for three representative periods of 12, 57, 128 min. The major induction anomalies that are indicated by observed induction arrows are explained below.

3.4. Induction Pattern

The real induction arrows with near WNW orientations at most of the sites indicate a massive conductivity anomaly causing SSW-NNE directed flow of induced currents somewhere on the north-western part. This induction pattern is coherent and the modulus of real induction arrows acquires a peak value around 57 min period. Further, given that induction effect maximizes when source field is polarized at WNW (−67.5°N), the spatial behaviour of real part of the anomalous induced field (Z_r) along the profile AA′ (Fig. 2b) is shown in Fig. 4a. Here, the real part of the anomalous vertical field (Z_r) induced by the source field of a unit amplitude and polarized N67.5°W at the period in question and at each station is estimated using the observationally reduced vertical field transfer functions, (T_{zx}, T_{zy}) as below:

$$Z_{r,i} = (T_{zx})\,r,\,i \;\times \cos\left(-67.5^{\circ}\right) + (T_{zy})\,r,\,i \times \sin\left(-67.5^{\circ}\right). \quad (3)$$

It is seen from Figs. 3 and 4a that the modulus of the real induction under this regional induction pattern, attains peak values at stations located on the northwestern periphery and decay rather slowly southeast landward to persist over a distance of

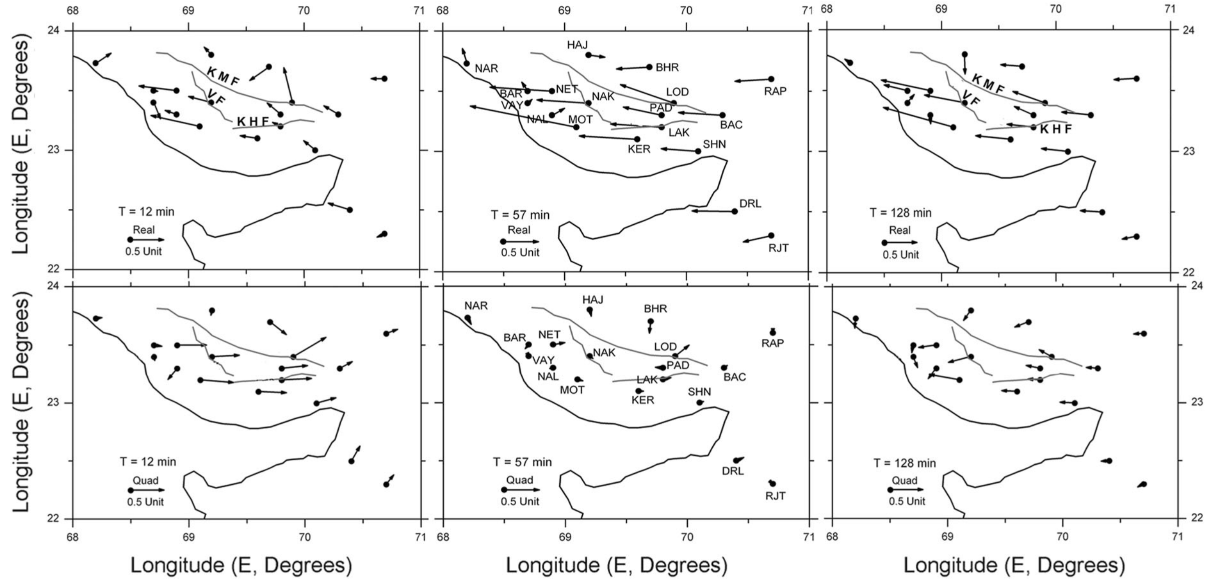

Figure 3

Sets of real and quadrature induction *arrows* for three periods superimposed on the geographic grid of the stations. Stations codes are in the *lower middle panel*

hundreds of kms. Both the location and decay pattern of the anomalous vertical fields are consistent with induction in an extended sheet like conductive structure. It can also be noted that at a period of around 57 min, the quadrature arrows have nearly vanishing amplitudes and their directions get reversed above and below this period. This critical period ($T_c = 57$ min) at which real arrows tend to acquire maximum amplitude and quadrature arrows flip their direction is characteristic of the anomalous body and can be used to estimate the longitudinal conductance (G, S) (Rokityansky 1982 and Chen and Fung 1987) defined as:

$$G = \sigma Q S = 5 \times 10^4 \times (T_c)^{1.2}\ \mathrm{S/m},$$

where σ is the conductivity (S/m) and Q is the cross sectional area (Q, m^2) of the anomalous conductivity body. Using the relation given above, the estimated longitudinal conductance of the anomalous conductivity structure is about 9.8×10^8 S/m. At periods well above and below the T_c, the quadrature arrows have modulus which are significant fractions of the accompanying real arrows, this demands that an associated sheet like structure, causing concentration of induced currents, is characterized by both resistance and self-inductance that would be generated by superficial sedimentary strata to the NW of the study area.

Annulling this regional trend, the real induction arrows at a group of stations (VAY, BAR and NAR) on the extreme western part of the study array shows a reverse trend and oppose the regional pattern dominated by WNW directed arrows. The oppositely directed arrows between two groups of stations, respectively having ESE and WNW orientations, are clear diagnostic of the concentration of the induced currents in an elongated structure running NE–SW. The vanishing magnitude of the real arrow at VAY signifies that the axis of the elongated structure causing concentration of the induced current is located right beneath these stations. Signature of the anomalous fields associated with this additional structure becomes apparent in Fig. 4b where estimated Z_r is plotted along the profile (BB′) cutting across the conductivity anomaly embedded between oppositely directed arrows (Fig. 3). Perhaps due to the superposition of the induction in an extended sheet and an elongated structure, the spatial variation of Z_r shows clear maxima and minima in close proximity to stations MOT and NAL. Drawing a line current analogy, the observed lateral extent between stations with extreme Z_r ($2d = \sim 25$ km) would

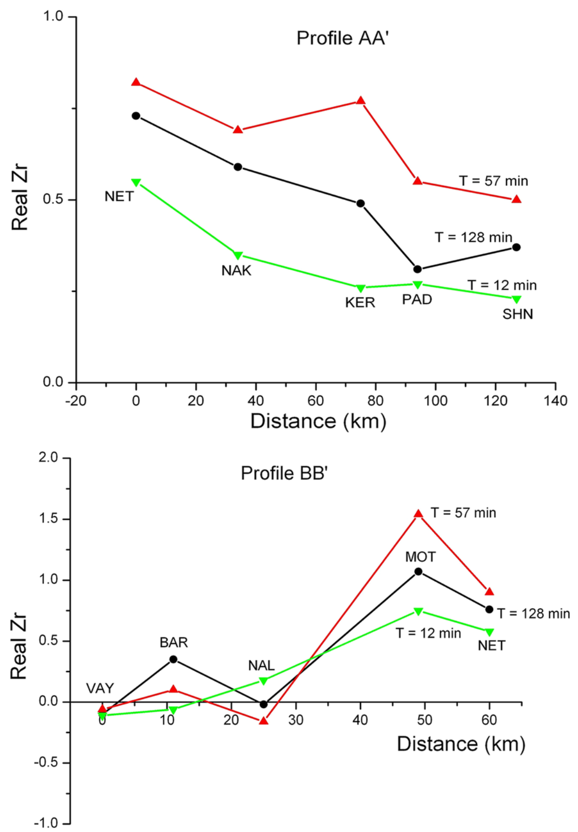

Figure 4
Plot of anomalous vertical induced field (Z_r) along the profiles AA′ and BB′. (see Fig. 2b for the location of the profiles)

place the elongated structure at a maximum depth (d) of 12–13 km. However, more realistic approximation on the finite width and thickness for the band of induced currents would place the source at a much shallower depth, well within the basement structure. Another notable induction feature is that, unlike the regional extended anomaly, the quadrature arrows for a group of stations associated with an elongated conductive structure have negligible amplitude compared to the large real arrows, suggesting involved structure is marked by high inductive reactance.

At a shorter period of 12 min, the smooth large-scale induction pattern is distorted and certain localized heterogeneities are indicted by a single or a pair of stations. The one notable feature around BHR and LOD, is that at both the stations real induction arrows are enhanced in amplitude and re-orient to indicate a complex conductivity distribution. To bring out the conductive features associated with the regional as well as local induction anomalies, the lateral conductivity distribution, compatible with observed real induction arrows at 12 min period are numerically modeled using non-uniform thin sheet approximation (Vasseur and Weidelt 1977).

4. Numerical Modeling

4.1. Choice of Thin Sheet Model

The above appraisal of induction anomalies suggests the presence of multiple conductive structures with varying dimensions and overlapping induction effects. It is also noted that at a couple of stations, the magnitude of the real induction arrows exceed one, which suggests that in addition to EM induction in individual conductive structures, the regional induced currents are mending their flow paths and channeled through narrow elongated structure (Jones 1983). Further, the coast effect, arising from the induction in highly conducting sea water in the deep ocean on the south-west of the KRB, is also expected to influence observed induction effects. Therefore, to model the induction effects in multiple conductive structures, the non-uniform thin sheet modeling approach is adopted to quantitatively estimate the depth integrated lateral conductivity distribution that accounts for the observed induction response. The formulation is preferred because it even permits one to account for channeling affects. The formulation considers all anomalies to be confined to a mathematically thin sheet of variable conductance (depth integrated conductivity). Physically, the thickness of a non-uniform sheet is determined by the electrical properties of the material constituting the sheet itself and electrically linked substratum, so that at the frequency of investigation the horizontal electric field remains constant over the thickness of the sheet (Weaver 1982).

4.2. Design Parameters of the Model

Consistent with the thick cover of Mesozoic–Triassic–Late Cretaceous sediments and an observation that some salient induction features are compatible with induction in superficial sedimentary structures, the thin sheet was assigned a thickness of 6 km that allowed the incorporation of conductivity variation associated with sedimentary fill as well as a seawater column. The computation of EM response for a given distribution of conductance was carried out using the thin sheet formulation developed by Vasseur and Weidelt (1977). Numerical solutions are worked out under the assumption that anomalous (observation) domain is surrounded by a normal structure. Since the present observational domain is surrounded by formations of contrasting conductivity, e.g., including sea-water, Rann of Kachchh and continental landmass, the effect of induction in such a variable conductivity environment is minimized by extending the limits of working domain sufficiently far from the actual observational domain (Mareschal *et al*. 1987). For the purpose of numerical computation, an extended area between 22°–25°N and 67°–72°E was chosen while observations are confined to a central block between 22.8°–23.8°N and 68.5°–71°E. With this, the normal structure bounding the entire working domain is represented by 200 S (equivalent to ∼50 m of seawater).

4.3. Electrical Substratum Beneath the Thin Sheet

On the consideration of skin-depth, the EM waves even at period of 12 min would penetrate to upper mantle depths, and; hence, computed EM response waves would be sensitive to resistivity distribution in crustal and upper mantle depths. Given this sensitivity, results of pilot LMT measurements (10–20,000 s) undertaken to probe the full thickness of the lithosphere in the Bhuj region, were used (Arora *et al.* 2002). In this pilot experiment, LMT fields were recorded at four sites extending across the meso-seismal zone (locations shown in Fig. 2a, b). As an illustration, Fig. 5 presents 1-D electric resistivity distribution obtained by the inversion of apparent resistivity (ρ_{yx}) and phase (Φ_{yx}) curve at the LMT site Lodai (Lat 69.9°N, Long. 23.4°E). A top low resistivity (3–5 Ωm) layer simulates 3 km thick sedimentary cover. Another distinctive feature of the resistivity-depth profile is the mid-crustal conductive layer in the depth range of 10–17 km. The presence of such a high conductivity layer is consistent with the minimum 1-D velocity structure (Mandal 2007). Both complimentary information could be explained by the presence of metamorphic fluids released by dehydration reactions (Muir-Wood and King 1993). Since generally the Moho is not a electrical discontinuity, the imaged conductivity interface in the depth range of 150 km can be related with the lithosphere-asthenosphere boundary. In the background of this information, a non-uniform thin sheet layer is considered to overlie a 3-layered 1-D structure having a resistivity of 200, 50 and 1,000 with a thickness of about 10, 7 and 130 km below which a uniform half space with 30 Ωm, simulates the asthenosphere.

4.4. Numerical Computation of Conductance Distribution

Having set the geoelectric and physical parameters of the thin sheet, for the purpose of numerical calculations, the selected working domain of 3° × 5° was divided into 60 × 100 cells with a grid interval of 5.5 km. Numerical solutions have been obtained for the following two sets of electrical conductance distribution in the non-uniform thin sheet.

4.5. Coast Effect

The aim of this set of computation was to make a quantitative estimate of the influence and extent of the coast effect on the land magnetometer sites arising due to concentration of induced currents in highly conducting sea water (Parkinson and Jones 1979). The lateral variation of conductance in the thin sheet corresponding to the oceanic part is determined by the seawater of variable depths (bathymetry). The thickness of the water column has been obtained from the bathymetry maps (Fig. 6) published by the Naval Hydrographic Office NHO (1977). The resistivity of seawater was taken to be 0.33 Ωm. The results of numerical calculation of the electromagnetic induction are superposed in Fig. 6 in the form of a real induction arrows pattern at 12 min. The most dominant feature is that the induction arrows in general are directed away from the landmass, pointing at a right angle towards the nearest deep ocean. The coast effect at most observational sites is weak and this behaviour can be reconciled to a large extent by slope

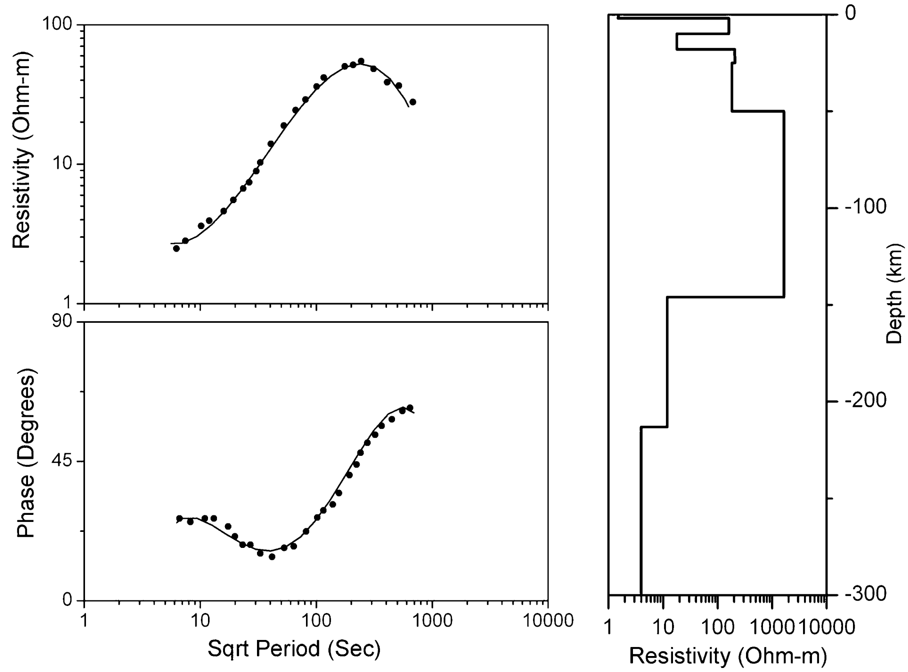

Figure 5
Left panels shows observed (*dots*) apparent resistivity and phase LMT sounding curves at site Lodai (LOD). *Smooth curve shows* model fit and the inverted resistivity-depth profile is shown in the *right panel*

geometry of the continental shelf region. Initially, on the SW, the bathymetry with 50 m seawater column, extends up to 100 km from the coast of Kachchh and then 200 m seawater column for another 100 km and the ocean-continental transition zone is located at a distance of more than 300 km from the west coast of India (Radhakrishna *et al*. 2002). The disagreement between the calculated coast effect and the observed induction arrows suggests the presence of a complex conductivity distribution on the continental part.

4.6. *Modeling of the Observed Induction Patterns*

As noted above, induction in sea water accounts for a very small fraction of the observed induction effects at the land magnetometer sites, the conductance distribution on the continental part was varied to explain the observed induction pattern in the KRB. In the basin environment, factors controlling the spatial distribution of conductivity includes permeability/porosity controlled degree of saturation, chemistry of water filling available porosity (e.g,. salinity), sediment facies (carbon, black shale, carbonates etc.) as well as overall variation in the thickness of the sedimentary column. Consistent with this, initial conductance distribution on the land part depicted spatial variations compatible with the surface geology as well as the tectonic trend. Noting that highland blocks (e.g. KMU, WU), which have undergone upliftment and folding and, thus, have thin Mesozoic sediment cover were assigned lower conductance in comparison to the plain areas filled with Tertiary and recent sediments (Banni plains). The vast saline watershed region of the Rann of Kachchh was simulated with moderately higher conductance roughly equivalent to 10 m of sea water. The computation of the depth-integrated conductance for each cell, in agreement with the MT studies (Sastry *et al*. 2008), surface sediments were assigned an average resistivity of 4 Ωm, whereas thickness estimates were adopted, constrained by MT, geophysical surveys and geological mapping. The conductance codes for nine classes of cells, simulating non-uniform thin sheet both on land and sea parts, are shown in Fig. 7. This initial conductance distribution was updated by a trial and error manner to reproduce major observed induction arrows, e.g., regional trend of WNW oriented arrows, reversal of

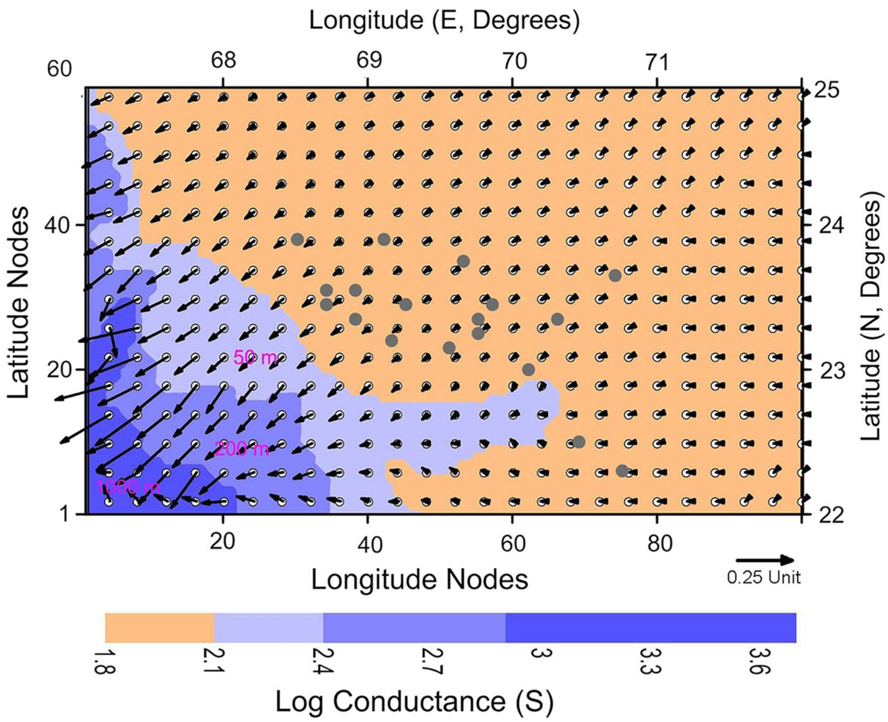

Figure 6
Conductance map showing variation of conductance in the ocean in accordance with the depth of sea water column (bathymetry) and uniform conductance on land part. The resulting induction *arrow* maps corresponding to period of 12 min and are shown for alternative grid. Magnetometer recording sites are shown by *circles*. *Colour* conductance index is shown separately

induction arrows between group of stations on the NW part of the array as well as select enhancement of arrows at individual or pair of stations. The skin-depth in the most conducting cell (12,000 S), represented by conductance code '*t*' in Fig. 7, exceeds the thickness of a non-uniform thin sheet and ensures linkage of the thin sheet with the substratum. Figure 8 shows the overall distribution of depth integrated conductance that reproduce the induction response close to the observed induction pattern (Fig. 9).

5. Results and Discussions

The spatial conductance distribution for the KRB, shown in Fig. 8 outlines five distinct anomalous zones, referred to as CA1, CA2,…, CA5. The sources of these anomalous zones may be seated in the upper sedimentary cover or in deep sub-surface structures. We discuss below their likely sources and generating mechanism together with the tectonic/seismotectonic implications.

5.1. Tectonic Implications

The tectonic setting of the KRB has been attributed to the reactivation of the Precambrian faults along the Delhi-Aravalli trend (Fig. 1) in the Early Jurassic (Biswas 1987). With the opening of the rift valley, the embayment between NPF and NKF was flooded with the Mesozoic sea during Middle Jurassic and a thick pile (~3,000 m) of marine sediments was deposited all over the KRB during a major cycle of sea transgression. Sea started regressing during Early Cretaceous due to a global sea level fall and upliftment of the trailing edge of the Indian plate as it tilted towards the Tethyan trench (Biswas 2005). During the Middle Jurassic transgression cycle, carbonate and shales were deposited, whilst deltaic clastics were deposited during the Late Jurassic to Late Cretaceous regressive cycle (Biswas

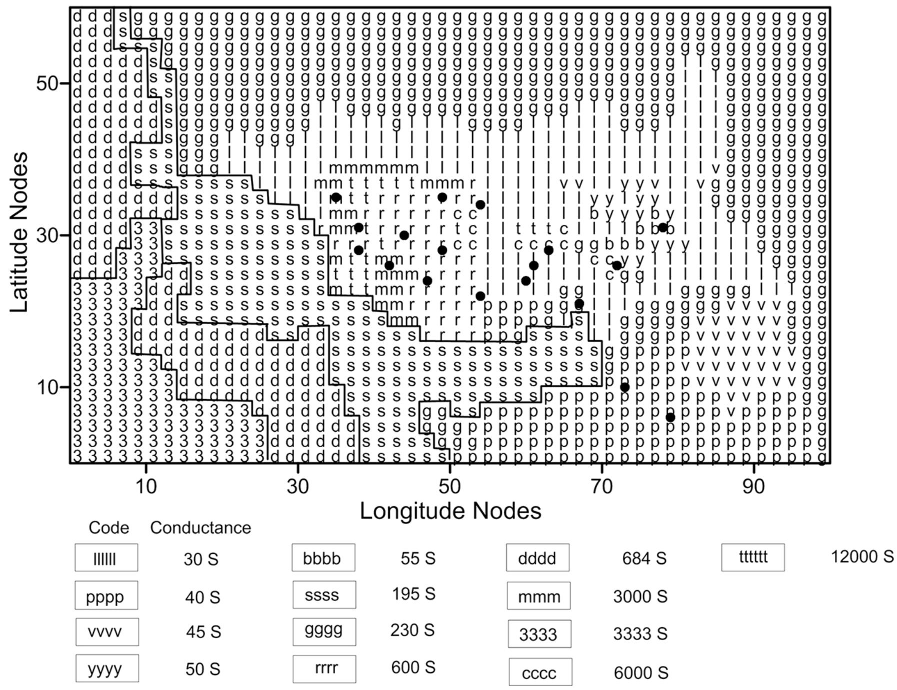

Figure 7
Conductance codes for the alternate working (60 × 100) nodes of the thin sheet model developed to define spatial distribution of depth-integrated conductance in and around the KRB as well as adjoining oceanic region. Conductance values for each character code and litho-sections determining the conductance for full thickness of the thin sheet are also shown

1991). As summarised in Sect. 2, the rift basin attained its present landscape following Late Cretaceous tectonic event that caused upliftment of fault bounded blocks in response to the large scale volcanic activity and widespread magmatic intrusions. The low lying plains sandwiched between uplands, formed sub-basins (Rann of Kachchh, Banni Plains, coastal belt of Gulf of Kachchh) for subsequent deposition during the post-rift sag stage. In addition to this Late Cretaceous mega event, Mishra *et al*. (2005) have emphasised the role of the triple junction of Indian, Arabian, and the Iranian plates, immediately west of the KRB, in the tectonic evolution of the KRB (Fig. 1). They noted that the Owen Fracture zone of Indian Ocean together with the Murray ridge is extending towards the continental shelf off the KRB, referred to as the Kachchh–Lakhpat lineament (KL, Fig. 1). This lineament (KL), immediately to the east, finds expression in bathymetry as a 35–40 km wide 'LOW' (Chauhan and Almeida 1993 also see Talwani and Gangopadhyay 2001), perhaps forming a gateway to the transgression of the sea beginning with Early Eocene transgression and subsequent Tertiary/Quaternary transgresive-regressive cycles.

On the premise that sea transgressions served as a channel for the influx of sediments and sediments attaining high electrical conductivity due to their sensitivity to chemical composition, fluid content etc. (possible mechanisms discussed in next section), the mapped conductivity anomalies can be used to locate thick depo-centres of sediments and/or even provide certain constrains on the pathways of sea invasion. It is inferred that after initial landward invasion up to the Lakhpat town, in line with bathymetry low, the paths of sea intrusion were controlled by structural low between Mesozoic uplifts. These sagging structural lows preserved the marine sediments deposited during the Mesozoic sea transgression and later developed into two first order embayment basins for the Tertiary sediments. Mapped ENE–WSW trending conductive zones CA1 and CA2 suggests that newly carved Banni half-Graben, formed following uplift of the KMU, provided seat for the deposition of

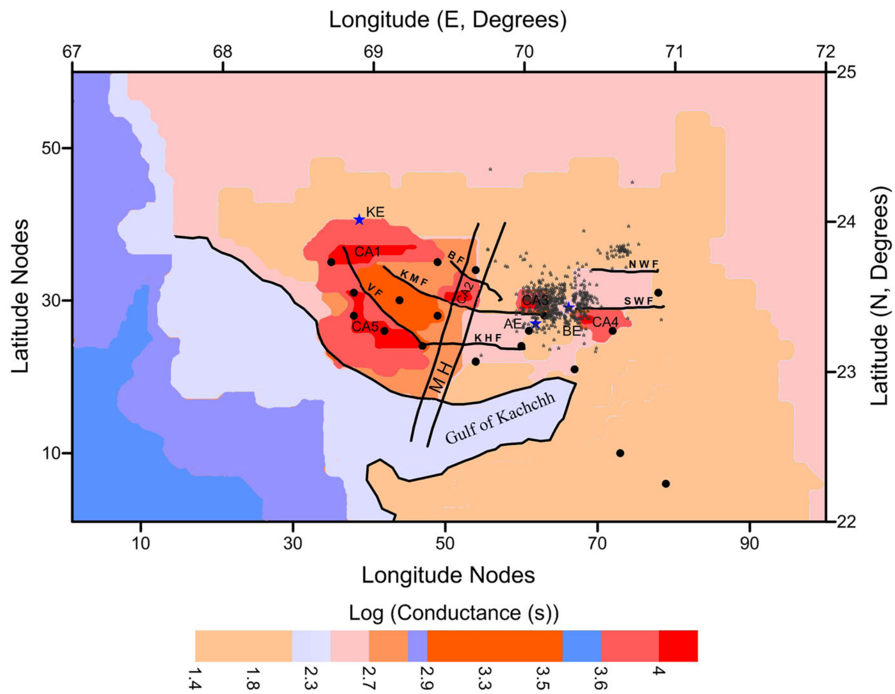

Figure 8
Spatial distribution in depth-integrated conductance in and around the KRB together with the mapped high conductivity anomalies, referred to as CA1, CA2,…, CA5. Different colour codes used to represent conductance values are in logarithms scale. The *grey dots* denote earthquakes recorded since 2001 Bhuj earthquake (after MANDAL and CHADHA 2008; SINGH *et al*. 2012)

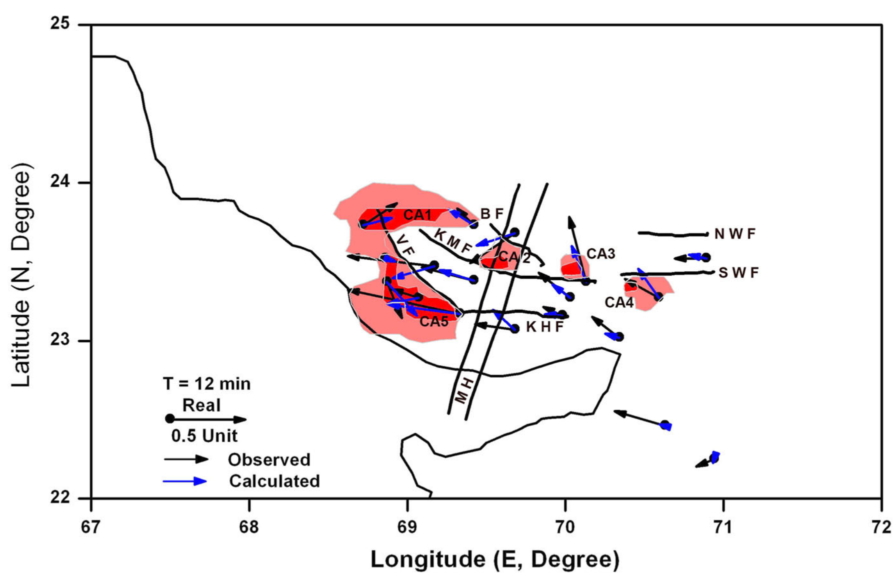

Figure 9
Comparison of observed and modelled real induction corresponding to period of 12 min in the background of mapped high conductance anomalous zones

sediments in association with a Late Eocene transgression. The dark shales were the major constituent of the deposited marine sediments whereas during the Middle Jurassic, carbonate and shales dominated the composition (BISWAS 1987). The control of the sea intrusion determining the sedimentation in the Banni graben has been emphasised by TALWANI and GANGOPADHYAY (2001). A seismic traverse across the basin has identified Banni Graben as an asymmetric half-graben with its axis near the KMF (SEDGELEY *et al.* 1997). Noting that its axis is co-linear with ENE–WSW trending bathymetry low on the continental shelf (Fig. 1), TALWANI and GANGOPADHYAY (2001) interpreted the bathymetry low as a channel for the influx of sediments to the Banni graben. SEDGELEY *et al.* (1997) independently noted that the axis of the Banni graben aligned with a chain of basins of Madagaskar, namely Diego, Majung and Morodnova basins. The large amplitude and orientation of induction arrows at BHR provided constraints on the geometry of the sedimentation in the Banni Graben. The large conductance accounting the large magnitude and southwesterly orientation of the induction arrow at BHR (Fig. 8) can be construed to indicate sedimentation in prismatic body with axis of maximum thickness immediately south of BF.

The mapped CA5 highlights an another structural low bounded between Vigodi fault and the westward extension of the KHF that served as channel for sea invasion and deposited marine sediments during the post-rift phase. Tracking the sedimentation history of the KRB, BISWAS (1987) observed that MH acts as a boundary across which the facies and thickness of the sediments show sharp transition. He also showed that on regional perspective, the MH can be viewed as a hinge zone that aligns with the hinge of the main Indus basin (Fig. 1). Further, noting a large asymmetry in the thickness of the Upper Jurassic-Lower Cretaceous sediments across the Median High, he indicated that the MH began to show regional bending during the Late Jurassic with a greater degree of subsidence and higher rate of sedimentation on its western flank. The CA5 west of the MH, paralleling the Vigodi fault, may represent the undisturbed section of the sediments deposited during the early phase of the basin evolution and later formed the seat for sedimentation during Tertiary sea transgression. The Banni graben is also tilted and deepens to the west of the MH. Higher depth integrated electrical conductance of CA1 compared to CA2 is consistent with larger thickness of sediments to the west of the MH.

5.2. *Possible Mechanisms for Enhanced Conductivity*

It has been shown above that mapped high conductivity zones (CA1, CA2 and CA5) are related to the tectonic evolution history during early phases. Since sediments deposited during early stage were basically carbonates and shales, the sedimentary sequences may owe the high conductivity to one or combination of the followings:

1. Presence of saline fluids
2. Shales rich sequences, even if they contain few meters of black shales or metamorphosed graphite schists, can account for the high conductance of the mapped conductive zones (DUBA *et al.* 1988).
3. The marine Mesozoic sediments have witnessed intensive igneous activity in the post-rift stage and were extensively intruded by Late Cretaceous magmatic intrusion. Aqueous fluid, released by recrystallizing magmatic bodies can contribute to the fluid budget and can be responsible for the enhanced conductivity (JIRACEK *et al.* 1979).
4. There also exists the possibility that high conductivity of the carbonate rich Lower Tertiary sequences may be a consequence of increased thermal effects associated with the Deccan volcanic activity. Laboratory measurements by BUCHA (1980) have shown that when hydrocarbon-saturated sedimentary formations are heated above a temperature of 200 °C, films of carbon are produced by pyrolysis reaction associated with diagenesis. Presence of carbon can enhance the electrical conductivity of the medium by several factors (DUBA *et al.* 1988). Presence of films of carbon and/or black shale may be the most potential candidates, especially for the CA5, is favoured by the following factors: (a) thin films of carbon on the grain boundary act as a carrier of electron and flow of induced currents in such a medium is marked by high inductive reactance, a property exhibited by the dominance of the real part over the quadrature part of induction arrows for a group of stations defining CA5 (see Sect. 3.4). (b) Generation of the carbon from carbonate rich sediments may be consequence of increased thermal effects associated syn-rift igneous activity or post-rift Deccan volcanic activity sourced by Reunion hotspot

plume. An equivalence of such a case can be drawn with the Parnaiba basin where the imaged high conductivity zone was attributed to the carbon-rich carbonates in the Cambro–Ordovician sequence preserved in the basement graben or thermally altered Paleozoic sediments in the central parts of the basin (Arora *et al*. 1999). Mesozoic sediments beneath the Deccan volcanic province have long been considered potential reserve for hydrocarbon (Satpal *et al*. 2006). A relevant question in respect of the imaged high CA5 is whether the hydrocarbon, if present, in the Mesozoic sediments preserved in the western flank of MH were destroyed during digenesis of the sediments due to overheating or driven off to an adjoining region, a mechanism proposed by Gombos *et al*. (1995) for the migration of hydrocarbon from the Surat depression to Bombay High. Recent discovery of hydrocarbon in Cretaceous and Jurassic in offshore Kachchh could be an example of this.

5.3. *Seimotectonic Implications*

Two localized conductivity anomalies CA3 and CA4 enclose the epicenter and the block defined by the concentrated aftershocks of the 2001 Bhuj earthquake (Fig. 8). Interestingly, the northern boundary of the high conductivity anomaly CA4 is cutoff by the Wagad upland. On the velocity tomograms, the Wagad upland from depth of 5 to 30 km (Mandal and Chadha 2008) is identified with high V_p and V_s. On the gravity and magnetic maps, the Wagad and other chain of Mesozoic uplands along the IBF are identified with localized and large amplitude positive anomalies (Mishra et al. 2005). These geophysical signatures favour plug-like mafic intrusives beneath the Wagad in association with intense Deccan volcanism. The aqueous fluids released from these recrystallizing mafic plugs could be the source of the presently mapped high conductivity zones CA3 and CA4. Fluid pressure from entrapped fluids in the CA3 and CA4 on the competent mafic intrusive could perturb the regional stress concentrations to produce frequent seismicity at shallow depth (<10 km). The hypothesis is similar to that inferred for the Valsad region where crustal adjustment of a volcanic plug embedded in the fluid-filled rock matrix (mapped as electrically conductive channel) was considered a source for localized seismic swarms (Arora and Reddy 1991, 2001). While such a geodynamic model explains the shallow aftershock activity, the seismotectonic model wherein it is proposed the underplated magmatic body immediately beneath hypocentral zone could have served as repository of high stresses while the fluid pressure in the fractured rock matrix above could have played key role in generating the 2001 Bhuj main shock and its prolonged aftershocks at deeper depths centered around 25 km (Biswas 2005; Mishra and Zhao 2003; Mishra *et al*. 2005; Mandal and Chadha 2008; Kayal 2010).

The integration of the present results with the previous MT studies in the KRB, brings home a central message that resistivity distribution, as a sensitive pointer of the fluid-related dynamics, can be used to constrain the earthquake nucleation and rupture processes. The presence of fluids induces rheological changes that modulate the mechanical and shear strength of the crustal rocks (Cox 2005) is abundantly evidenced by the resistivity space-depth distribution of the resistivity in the KRB. First, the source zone of the Bhuj earthquake is rooted in the sharp resistivity-conductivity interface (Chandrasekhar and Harinarayana 2012). Second, magnetotelluric measurements show the presence a high conductive (low resistivity) in mid-crustal (10–17 km) depths (Arora *et al.* 2002; Sastry *et al*. 2008). Incorporation of fluid induced ductile layer in the crustal section could explain bi-focal distribution of hypocentres seen in the meso-seismal zone (Mishra *et al*. 2008), i.e., plug-like mafic intrusion in the brittle upper crust and compact underplated magamatic body around 25 km depth serve as stress concentrators which under fluid-pressure from enclosing rock matrix generate frequent seismicity including the 2001 Bhuj earthquake. This validates the tectonic model of KRB derived from the seismotectonic (Mandal 2012) and geological data (Biswas 2005).

6. *Conclusions*

The processing and modelling of transient geomagnetic variations recorded by a regional scale magnetometer array reveal flow paths of concentrated induced currents associated with zones of enhanced electrical conductivity. Decomposition of induction response into real and quadrature parts favour the observed induction resulting from surface sedimentary strata. Given the role of sea transgression in sedimentation, the mapped conductivity anomalies are related to the relics of thick depo-centres of sediments, the black shale, carbonate coupled with saline fluids content accounting for the high conductivity. Accepting this connotation, spatial distribution of the mapped conductivity anomalies suggests that sea invasion controlled sedimentation, after entering the land through off-shore bathymetry 'LOW', were guided by the structural low along the Banni Graben, immediately north of the Kachchh Main fault, as well as along the Vinjan depression, west of the Vigodi fault. These post Mesozoic Tertiary structural reliefs are still maintained by the neotectonic activity continuing since the Late Cretaceous rift inversion due to the present regional compressive stress on the Indian plate (Biswas, personal communication).

In addition to the conductivity anomalies related with the tectonic evolution of the KRB, two localized anomalies are mapped enclosing the block defined by the 2001 Bhuj earthquake and its aftershocks. A model is suggested wherein fluid pressure entrapped within high conductivity/low velocity zones perturb the stresses accentuated near the surface volcanic plugs and a deep seated magmatic body to generate earthquakes and their bi-focal depth distribution. This conclusion is compatible with the seismotectonic and geological interpretations.

Acknowledgments

The design of the experiment and interpretation of results were greatly benefitted by extensive discussions with Drs S.K. Biswas and C.D. Reddy, which are gratefully acknowledged. In the initial stages, Dr R.V. Karanth was kind to guide us through field excursion and introduced us to the geology of the area. Drs S.K. Biswas and S. Chopra critically read the manuscript and made many useful suggestions for improvements. Drs D.C Mishra, O.P. Mishra, P. Mandal and A.P. Singh readily made available their research publications, which enriched our understanding of the geodynamics of the region. Help of all these colleagues is deeply appreciated and acknowledged. Authors thank the Head of the host Institutions for their encouragement and support. One of us (BRA) thank the CSIR and the MoES for providing facilities, financial support and encouragement, which enabled him to complete the work presented here. The authors place on record their appreciation for state officials, teachers, and farmers who not only provided space to house the magnetometers but also provided help in smooth operation of the experiments.

References

Arora, B.R. (1997), *Geomagnetic depth sounding*. In: Arora, B.R. and Sriniwas (Eds), Natural source electromagnetic induction in the earth, New age international publishers Ltd, New Delhi, pp. 80–128.

Arora, B.R. and Reddy, C.D. (1991), *Magnetovariational study over a seismically active area in the Deccan trap province of western India.* Phys. Earth Planet. Intr., *66*, 118–131.

Arora B.R. and Reddy C.D. (2001), *Correlation between high electrical conductivity and seismicity: role of fluids*. Ind. Geol. Congress, *1*, 267–276.

Arora, B.R., Gautam Rawat and Singh, A.K. (2002), *Mid-crustal conductor below the Kutch rift basin and its seismogenic relevance to the 2001 Bhuj earthquake*. DCS-DST News letter, *12*, 22–24.

Arora, B.R., Padilha, A.L., Vitorello, I., Trivedi, N.B., Fontes, S, Rigoti, A. and Chamalaun, F.H. (1999), *2-D geoelectrical model for the Parnaiba basin conductivity anomaly, north-northeast Brazil and its tectonic implications.* Tectonophysics, *302*, 57–69.

Beamish, D. (1977), *The mapping of Induced currents around the Kenya rift: a comparison technique.* Geophys. J. Royal Astron. Soc., *50*, 311–322.

Bilham, R., Bendick, R. and Wallace, K. (2003), *Flexure of the Indian Plate and Intraplate Earthquakes.* Proc. Indian Acad. Sci. (Earth Planet Sci.), *112*, 1–14.

Biswas, S.K. (1982), *Rift basins in western margin of India with special reference to hydrocarbon prospects.* Bull. Am. Assoc. Petrol. Geol., *66*, 1497–1513.

Biswas, S.K. (1987), *Regional tectonic framework, structure and evolution of the western marginal basins of India*. Tectonophysics, *135*, 307–327.

Biswas, S.K. (1991), *Stratigraphy and sedimentary evolution of Mesozoic basin of Kutch*. In: Tandon, S.K., Pant C.C. and Casshyap, S.M. Sedimentary basins of India, Gyanodaya Prakashan, Nainital, pp. 74–103.

Biswas, S.K. (2005), *A review of structure and tectonics of Kutch basin Western India.* Curr. Sci., *88*(10), 1592–1600.

Biswas, S.K. and Khattri, K.N. (2002), *A geological study of earthquakes in Kutch, Gujarat, India*. J. Geol. Soc. India, *60*, 131–142.

Bucha, V. (1980), *Geomagnetism of the external flysch Czechoslovakian Carpathians and the possible causes of the anomalous geophysical manifestations*. Stud. Geophys. Geod., *24*, 227–251.

Byerlee, J.D. (1990), *Friction, overpressure and fault normal compression*. Geophys. Res. Lett., *17*, 2109–2112.

Chandrasekhar, E., George Mathew and Harinarayana, T. (2012), *A new hypothesis for the deep subsurface structures near the Bhuj 2001 earthquake (Mw 7.6) hypocenter zone and its tectonic implications*. Geophys. J. Int., *190*, 761–768.

Chauhan, O.S. and Almeida, F. (1993), *Influences of Holocene sea level, regional tectonics and fluvial, gravity and slope currents induced sedimentation on the regional geomorphology of the continental slope off northwestern India.* Mar. Geol., *112*, 313–328.

Chen, P.F. and Fung, W. (1987), *On the behavior of the imaginary Parkinson arrows near the anomalous conductive–host medium interface.* Phys. Earth Planet. Inter., *50*, 195–198.

Cox, S.F. (2005), *Coupling between deformation, fluid pressures, and fluid flow in ore producing hydrothermal systems at depth in the crust.* In: Hedenquist, W., Thompson, J.J. and Goldfarb, R.R. (Eds.), Economic Geology, 100th Anniversary Volume, pp. 39–76.

Duba, A., Huenges, E., Nover, G. and Will, G. (1988), *Impedance of black shale from the Munsterland I borehole: an anomalously good conductor.* Geophys. J Int., *94*, 413–419.

Gombos, A.M. Jr, Powell, W.G. and Norton, I.O. (1995), *Tectonic evolution of western India and its impact on hydrocarbon occurrences: an overview*. Sed. Geol., *96*, 119–129.

Gowd, T.N., Rao, S.V.S. and Chary, K.B. (1996), *Stress field and seismicity in the Indian shield: effects of the collision between India and Eurasia.* Pure Appl. Geophys., *146*, 503–531.

Gupta, H.K., Harinarayana, T., Kousalya, M., Mishra, D.C., Mohan, I., Purnachandra Rao, N., Raju, P.S., Rastogi, B.K., Reddy, P.R. and Sarkar, D. (2001), *Bhuj earthquake of 26 January 2001*. J. Geol. Soc. India, *57*, 275–278.

IIG Working Group for Bhuj Earthquake Related Studies (2002), *Geophysical investigations in the January 6, 2001 Bhuj Earthquake affected region*, In: Proceedings of the workshop on Recent Earthquakes of Chamoli and Bhuj, II, May 24–26, 2002.

Jiracek, G.R., Ander, M.E. and Holcombe, H.T. (1979), *Magnetotelluric soundings of crustal conductive zones in major rifts*. In: Robert E.R. (Ed), Riogrande Rift: Tectonics and magmatism. American Geophysical Union, Washington DC, pp. 209–222.

Jones, A.G. (1983), *The problem of current channeling: critical review*. Geophys. Surv., *6*, 79–122.

Kayal, J.R. (2007), *Recent Large Earthquakes in India: Seismotectonics Perspective*. IAGR Memoir No., *10*, 189–199.

Kayal, J.R., De, Reena, Ram, S., Srirama, B.V., and Gaonkar, S.G. (2002a), *Aftershocks of 26 January 2001 Bhuj Earthquake in Western India and its Seismotectonic Implications*. J. Geol. Soc. India, *59*, 395–417.

Kayal, J.R., Zhao, D., Mishra, O.P., De, R. and Singh, O.P. (2002b), *The 2001 Bhuj earthquake: Tomographic evidence for fluids at the hypocenter and its implications for rupture nucleation*. Geophys. Res. Lett., *29*, 5.1–5.4.

Kayal, J.R., Das, Vishal, and Ghosh, Uma, (2010), *An appraisal of 2001 Bhuj earthquake (Mw 7.7) source zone: Fractal dimension and b-value mapping of the aftershock sequence*. Pure Appl. Geophys., *167*(11), 1303–1458.

Kukowski, N., Schilhorn, T., Huhn, K., Von Rad, U., Husen, S. and Flueh, E.R. (2001), *Morphotectonics and mechanics of the central Makran accretionary wedge of Pakistan.* Mar. Geol., *173*, 1–19.

Lilley, F.E.M. and Arora, B.R. (1982), *The sign convention for quadrature Parkinson arrows in geomagnetic induction studies.* Rev. Geophys., *20*, 513–518.

Mandal, P. (2007), *Sediment thicknesses and Qs vs. Qp relations in the Kachchh rift basin, Gujarat, India using Sp converted phases*. Pure Appl. Geophys., *164*, 135–160.

Mandal, P., (2012), *Passive-Source Seismic Imaging of the Crust and Upper Mantle beneath the 2001 Mw 7.7 Bhuj Earthquake Region, Gujarat, India.* Bull. Seismo. Soc. Am., *102*(1), 252–266.

Mandal, P. and Chadha, R.K. (2008), *Three-dimensional velocity imaging of the Kachchh seismic zone, Gujarat, India,* Tectonophysics, *452*, 1–16.

Mandal, P., Rastogi, B.K., Satyanarayana, H.V.S. and Kousalya, M. (2004), *Results from Local Earthquake Velocity Tomography: Implications toward the Source Process Involved in Generating the 2001 Bhuj Earthquake in the Lower Crust beneath Kachchh (India)*. Bull. Seism. Soc. Am., *94*, 633–649.

Mareschal, M., Vasseur, G., Srivastava, B.J., Singh, R.N. (1987), *Induction models of southern India and effect of offshore geology.* Phys. Earth Planet. Inter., *45*, 137–148.

Mishra, D.C., Chandrasekhar, D.V. and Singh, B. (2005), *Tectonics and crustal structures to Bhuj earthquake of January 26, 2001: based on gravity and magnetic surveys constrained from seismic and seismological studies.* Tectonophysics, *396*, 195–207.

Mishra, O.P. and Zhao, D. (2003), *Crack density, saturation rate and porosity at the 2001 Bhuj, India, earthquake hypocenter: a fluid-driven earthquake?* Earth Planet. Sci. Lett. *212*, 393–405.

Mishra, O.P., Zhao, D. and Wang, Z. (2008), *The genesis of the 2001 Bhuj, India earthquake (Mw 7.6): a puzzle for peninsular India?* Indian Miner., *61*, 149–160.

Muir-Wood, R. and King, G.C.P. (1993), *Hydrological signatures of Earthquake strain*. J. Geophys. Res., *98*, 22035–22068.

NHO. (1977), Bathymetry *map of Bay of Bengal*. Superintendent, Naval Hydrographic Office, Dehradun, India.

Parkinson, W.D. and Jones, F.W. (1979), *The geomagnetic coast effect*. Rev. Geophys. Space. Phys., *17*, 1999–2011.

Radhakrishna, M., Verma, R.K. and Purushotham, A.K. (2002), *Lithospheric structure below the eastern Arabian Sea and adjoining west coast of India based on integrated analysis of gravity and seismic data.* Mar. Geophys. Res., *23*, 25–42.

Rokityansky I.I., (1982), *Geomagnetic investigations of the Earth's crust and mantle*. Springer Verlag, Berlin, Germany.

Satpal, Singh, O.P., Sar, D., Chatterjee, S.M. and Sanjeev Sawai (2006), *Integrated interpretation for sub-basalt imaging in Saurashtra Basin, India.* The leading Edge, *26*, 881–885.

Sastry, R.S., Nandini N. and Sarma, S.V.S. (2008), *Electrical imaging of deep crustal features of Kachchh, India*. Geophys. J. Int., *172*, 934–944.

Schmucker, U. (1970), *Anomalies of geomagnetic variations in the southwest United States*, Bull. Scripps Inst. Oceanog., *13*, 1–165.

Sedgeley, D., Yawanarajah, S. and Bastia, R. (1997), *Petroleum potential of the Banni graben, Kutch basin*. AAPG Bull., *81*, 1411.

Singh A.P., Mishra, O.P., Yadav, R.B.S. and Kumar, D. (2012), *A new insight into crustal heterogeneity beneath the 2001 Bhuj earthquake region of northwest India and its implications for rupture initiations.* J. Asian Earth Sci., *48*, 31–42.

Talwani, P. and Gangopadhyay, A. (2001), *Tectonic frame work of the Kachchh Earthquake of 26 January 2001*. Seismol. Res. Lett., *72*, 337–345.

Vasseur, G. and P. Weidelt. (1977), *Bimodal electromagnetic induction in nonuniform thin sheets with an application to the northern Pyrenean induction anomaly.* Geophys. J. R. Astron. Soc., *51*, 669–690.

Weaver, J.T. (1982), *Regional induction in Scotland; and example of three-dimensional numerical modeling using the thin sheet approximation.* Phys. Earth Planet. Inter., *28*, 161–180.

(Received August 17, 2013, revised February 24, 2014, accepted April 4, 2014, Published online May 1, 2014)